Infrared Spectroscopy Reveals Metal-independent Carbonic Anhydrase Activity in Crotonyl-CoA Carboxylase/Reductase

Aharon Gomez[1†], Matthias Tinzl[2†], Gabriele Stoffel[2], Helmut Grubmüller[3], Tobias J. Erb[2,4], Esteban Vöhringer-Martinez[1*], Sven T. Stripp[5*]

[1]Departamento de Físico Química, Facultad de Ciencias Químicas, Universidad de Concepción, Concepción, Chile;

[2]Department of Biochemistry and Synthetic Metabolism, Max-Planck-Institute for Terrestrial Microbiology, Karl-von-Frisch-Str. 10, D-35043 Marburg, Germany;

[3]Department of Theoretical and Computational Biophysics, Max-Planck-Institute for Biophysical Chemistry, Am Fassberg 11, 37077 Göttingen, Germany;

[4]Center for Synthetic Microbiology (SYNMIKRO);

[5]Freie Universität Berlin, Experimental Molecular Biophysics, Arnimallee 14, 14195 Berlin, Germany

† These authors contributed equally
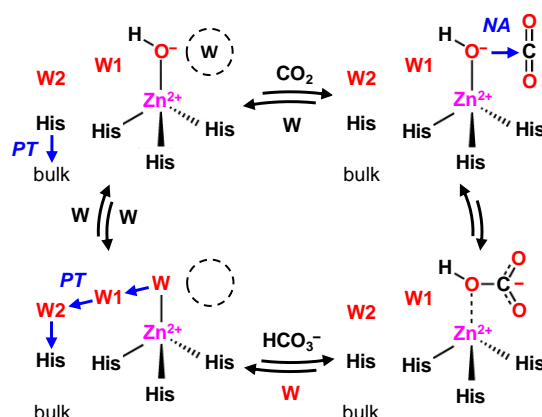
Email: evohringer@udec.cl, sven.stripp@gmail.com

Abstract

The conversion of CO_2 by enzymes such as carbonic anhydrases or carboxylases plays a crucial role in many biological processes. However, methods to study the conversion of CO_2 at the active site of enzymes *in situ* are still limited. Here, we used Fourier-transform infrared (FTIR) spectroscopy to study the interaction of CO_2 with crotonyl-CoA carboxylase/reductase from *Kitasaospora setae* (*Ks*Ccr), one of the fastest CO_2-fixing enzymes in nature. Our studies reveal that the enzyme possesses a so far unknown metal-independent carbonic anhydrase activity. Molecular dynamics (MD) simulations explain why substrate binding inhibits anhydrase activity, and mutations of active site residues of *Ks*Ccr suggest that an 'activated' water molecule, coordinated by a histidine and glutamate residue, forms the hydroxyl anion that attacks the CO_2 molecule. Altogether, we demonstrate how *in situ* FTIR spectroscopy combined with MD simulations provides new means to investigate the interaction of different proteins with CO_2, providing a simple, yet powerful approach to atomistic reaction mechanisms including CO_2 hydration and enzymatic (de-)hydration reactions.

Introduction

Developing catalytic strategies for the capture and conversion of carbon dioxide (CO_2) is key to increased mitigation, utilization, and sequestration of this important greenhouse gas. While still being a challenge for synthetic chemistry, enzymes provide a natural blueprint for efficient CO_2-converting catalysts. Several enzymes are known that interact with CO_2 and/or bicarbonate (HCO_3^-) during catalysis, in particular carbonic anhydrases (CAs) and carboxylases.
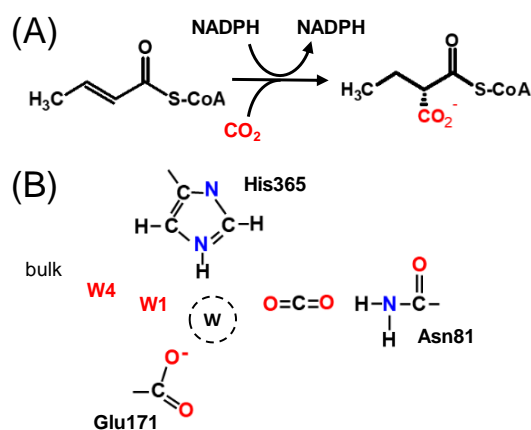
CAs catalyze the reversible interconversion of CO_2 and HCO_3^- with rate enhancements of close to $8x10^6$ compared to the reaction in aqueous solution. This makes them one of the most effective CO_2-converting catalysts in nature.[1] CAs are present in all three domains of life and have been classified in eight families.[2] Almost all known family members feature a zinc cation at their active site, which plays a central role in catalysis (**Scheme 1**): the cation coordinates a hydroxide anion (OH^-), which attacks CO_2 as a nucleophile to form HCO_3^-. The OH^- species itself is generated through a proton transfer from a zinc-bound water molecule to a proton acceptor, which is usually a histidine.[3–6]

Scheme 1. Mechanism of CO_2 hydration in carbonic anhydrase. CO_2 enters the active site and replaces a water molecule (W, black) near the zinc ion. In the next step, CO_2 is converted to HCO_3^- upon a nucleophilic attack (NA) of the zinc-bound hydroxide (Zn^{2+}-OH^-). At the zinc site, HCO_3^- is replaced by a water molecule (W, red), the latter which is activated to OH^- upon proton transfer (PT) *via* crystal water W1 and W2 and a conserved histidine. In the last step, histidine changes its orientation to release the proton into bulk solvent, and water re-binds at the active site. After Kim *et al.* [6].

Carboxylases capture and catalyze the addition of CO_2 to an acceptor substrate, and the recently discovered family of enoyl-CoA carboxylases/reductases (ECRs) encompasses some of the most efficient CO_2-fixing enzymes found in nature.[7] ECRs catalyze the reductive carboxylation of α,β-unsaturated enoyl-CoAs with the reduced form of nicotinamide adenine

dinucleotide phosphate (NADPH) as cofactor (**Scheme 2A**). Hydride transfer from NADPH to the enoyl-CoA substrate generates a reactive enolate species, which acts as a nucleophile that attacks a CO_2 molecule bound at the active site.[8,9] **Scheme 2B** illustrates how CO_2-binding in ECRs is achieved through four amino acid residues and one conserved water molecule that is coordinated by two conserved active site residues, an aspartate and a histidine.[10]

Scheme 2. Mechanisms of CO_2-fixation in carboxylase/reductase. (A) *Ks*Ccr catalyzes the NADPH-dependent carboxylation of crotonyl-CoA (left) into ethylmalonyl-CoA (right). **(B)** *Ks*Ccr active site residues H365, E171, and N81 that interact with CO_2 during the carboxylation reaction. W refers to a water molecule between H365 and E171, W1–W4 from a local water cluster that connects the active site with bulk solvent.

All molecular species involved in the above described CO_2-conversions (H_2O, CO_2, HCO_3^-) show characteristic absorbance in the infrared, which makes them available to Fourier-transform Infrared (FTIR) spectroscopy.[11–14] In a protein sample, however, these signals are overlaid by the intense absorbance of bulk water and the amide bands of the protein backbone.[15] This limitation can be overcome by FTIR difference spectroscopy, which provides the means to distinguish between protein sample background signals and the signature of a given reaction upon a specific trigger.[16] We recently developed a FTIR difference spectroscopy-based setup in which catalysis can be triggered *via* the gas phase.[17] Compared to the conventional transmission configuration, a protein film is formed on top of the silicon crystal of an attenuated total reflection (ATR) optical cell[18], which makes the protein amendable to changes in the gas phase, *e.g.*, by switching from a 'carrier gas' (100% N_2 or Ar, defining the background signal) to a 'reactive' gas mixture. This specific design allows studying the reaction of CO_2-converting enzymes, providing the substrate (*i.e.,* CO_2) *in situ* and thus the reaction trigger for these enzymes.[17]

Here, we applied *in situ* ATR FTIR spectroscopy to study the interaction of a well-established model ECR with CO_2, namely crotonyl-CoA carboxylase/reductase from *Kitasaospora setae* (*Ks*Ccr).[10] Our results show that the active site of *Ks*Ccr does not only bind CO_2, but surprisingly also possesses a so-far unknown, intrinsic ('hidden') CA activity, which enables the enzyme to catalyze the reversible conversion of CO_2 and HCO_3^-. Studying the reaction in absence or presence of substrates or inhibitors with wild-type and four active site variants, we identified key residues for the observed CA activity, including a cluster of strongly hydrogen-bonded water molecules. Moreover, computer simulations suggest that conformational dynamics and substrate binding in *Ks*Ccr modulate CO_2 binding at the active site and thus influence CA activity. Combining experiment and simulation, we propose a mechanism for *Ks*Ccr CA activity that involves the conserved, activated water molecule, which is essential for CO_2-binding during the CO_2-fixation reaction of *Ks*Ccr, but also serves as nucleophilic OH^- anion in the enzyme's CA reaction.

Results and Discussion

Infrared Signatures of Anhydrase Activity

To probe the reaction of *Ks*Ccr with CO_2, we prepared a protein film from 1 µl *Ks*Ccr solution (200 µM) on the silicon crystal of an ATR cell and monitored water evaporation by FTIR spectroscopy *in situ*. We rehydrated the protein film under a stream of aerosol (3 L/min) that was created by sending dry N_2 gas through a wash bottle containing a dilute Tris/HCl buffer solution (1 mM, pH 8). Once the *Ks*Ccr protein film was rehydrated, we added 10% CO_2 to the gas flow for 50–100 s and recorded data to calculate a series of *in situ* FTIR difference spectra of the interaction of *Ks*Ccr with CO_2 (**Figure S1**).

Figure 1A depicts such a 'CO_2–N_2' FTIR difference spectrum, recorded 25 s after addition of CO_2. The positive band at 2342 cm^{-1} corresponds to CO_2 in solution.[11] Further positive bands were observed at 1618 cm^{-1}, 1358 cm^{-1}, and 1258 cm^{-1}, the latter as a shoulder. These bands were assigned to the asymmetric and symmetric stretching modes of CO_2 (v_2, v_3) as well as the COH bending mode (v_4) of bicarbonate in solution[12–14], which surprisingly indicated that *Ks*Ccr had catalyzed formation of HCO_3^-. A broad negative band at 3020 cm^{-1} appeared in an energy regime corresponding to a strongly hydrogen-bonded network of 'local' water molecules[19–21], indicating that water is consumed during bicarbonate formation. Besides these strong signals, the FTIR difference spectrum also showed unspecific hydration changes (**Figure S2**) resulting in a minor increase of bulk water (sum of OH stretches at ~3320 cm^{-1}) and minor decrease of amide bands (amide I at ~1660 cm^{-1} and amide II at ~1540 cm^{-1}).[15]

To confirm assignment of the observed bands, we investigated potential isotope effects. Adding $^{13}CO_2$ gas instead of CO_2 resulted in a specific down-shift of the CO_2 band to 2278 cm^{-1} (Δ64), as well as the v_2 and v_3 bands to 1586 cm^{-1} and 1322 cm^{-1} (Δ32 and Δ36), respectively. The isotope effect on the band at 1258 cm^{-1} was rather minor, while the broad negative band at 3020 cm^{-1} was not affected by the $^{13}CO_2$ isotope, which is in line with our assignments of CO_2/bicarbonate and the water cluster. We also investigated the influence of solvent isotope effects by exchanging the hydrated KsCcr protein film from H_2O to D_2O (**Figure 1B**). In D_2O, we observed a large down-shift of the negative band from 3020 cm^{-1} to 2280 cm^{-1} (Δ740), supporting our assignment of the water cluster. While the H/D exchange had only insignificant effect on the v_2 and v_3 bands, the shoulder at 1298 cm^{-1} seemed to disappeare in the deuterated sample. This is due to a ~300 cm^{-1} shift to lower frequencies confirming the COH (v_4) assignment .[13]

We next used our ATR FTIR setup to study the kinetics of the KsCcr reaction with CO_2. To this end, we fitted difference spectra with abovementioned contributions, corrected for unspecific changes, and plotted the resulting 'peak area' against time (**Figure S2**). This approach provided apparent time constants (τ_{app}) representing the reaction velocity at which the system converged to steady-state conditions. **Figure 1C** shows the changes of the HCO_3^- bands (shown here as a combination of v_2, v_3, and v_4) and the water cluster band in KsCcr upon reaction with 10% CO_2 followed by 100% N_2. Over five cycles, we found the CO_2/HCO_3^- conversion to be reversible, with the back reaction approximately five times slower compared to the forward reaction (τ_{app} = 125 s ±10.1 and 26.4 s ±1.66, see **Figure S3**). We also titrated KsCcr in five consecutive steps with 1–100% CO_2 (**Figure 1D**) resulting in an exponential decrease of τ_{app} from 47 ±6.1 s (1% CO_2) to 5.6 ±0.4 s (100% CO_2), which demonstrated that the conversion reaction is CO_2-dependent (**Figure S3**). Compared to Na_2CO_3 in aqueous solution, these data allow for quantification of bicarbonate conversion *via* the v_3 band at 1358 cm^{-1} (**Figure S1**) so that a bicarbonate formation velocity can be defined. Plotted against CO_2, we determined Michaelis-Menten parameters V_{max} = 0.17 ±0.01 µM HCO_3^- s^{-1} and K_m = 19 ±3.1% CO_2 for the CO_2 hydration reaction (**Figure S3**).
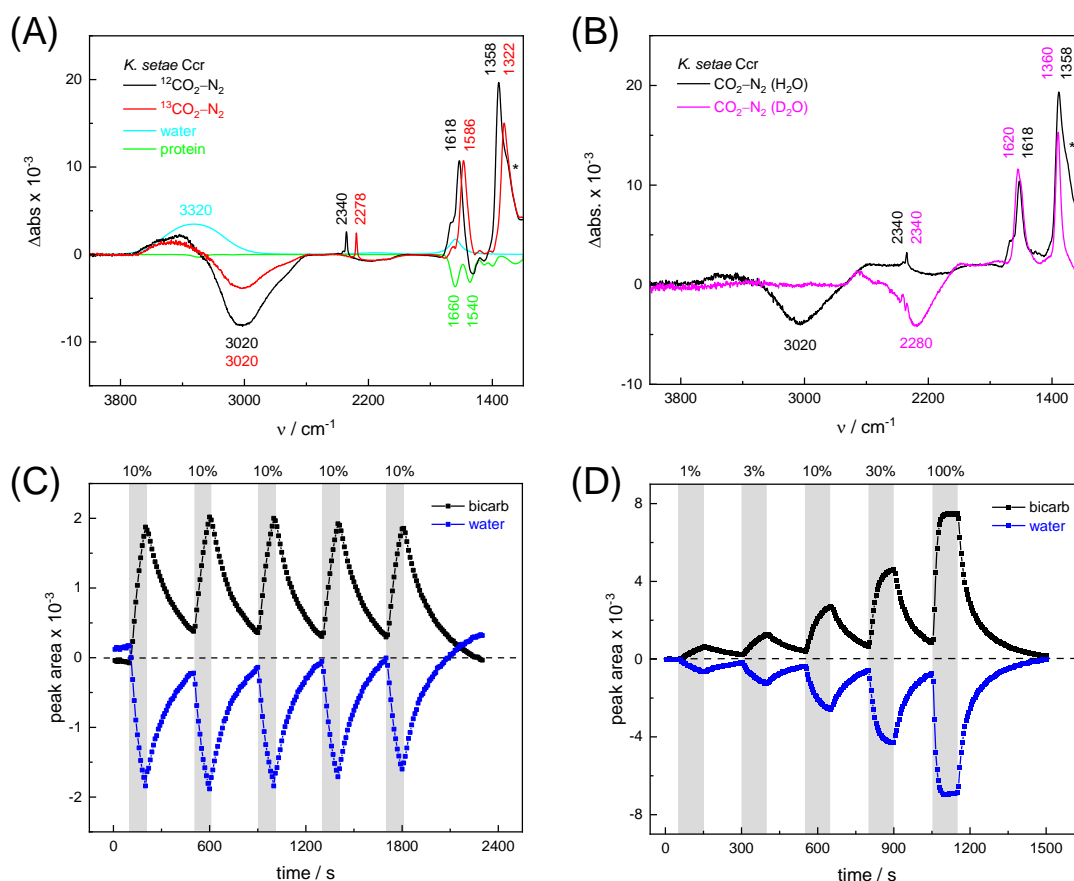
Figure 1 | Infrared characterization of the reaction of *Ks*Ccr with CO_2. **(A)** 'CO_2–N_2' ATR FTIR difference spectra for the reaction with $^{12}CO_2$ (black) or $^{13}CO_2$ (red). Fits depict unspecific changes in hydration level (cyan, liquid H_2O) and protein concentration (green, mainly amide I and II) that shape the spectrum. Positive signals are assigned to CO_2 (2340 or 2278 cm^{-1}) and bicarbonate. The COH vibration (v_4) appears at 1298 cm^{-1} (*). **(B)** 'CO_2–N_2' ATR FTIR difference spectra in the presence of H_2O (black) or D_2O (magenta). The broad negative bands are assigned to 'local' H_2O (3020 cm^{-1}) or D_2O (2280 cm^{-1}). **(C)** Evolution of the bands assigned to HCO_3^- (black) and the water band at 3020 cm^{-1} (blue) over time in the presence of 10% CO_2 (grey area) or 100% N_2. The data highlight the reversibility of the reaction. **(D)** The CO_2 partial pressure (1–100%) affects the intensity of difference signals and reaction velocities. See Supporting Information for further analyses.

To verify and benchmark the CO_2/HCO_3^- conversion by *Ks*Ccr, we repeated the experiments with the β-type CA from *E. coli* (*Ec*CA)[22] at conditions comparable to the experiments with *Ks*Ccr (**Figure S4**). The CO_2–N_2 FTIR spectrum for *Ec*CA after 25 s (**Figure 2A**) is strikingly similar to the one observed for *Ks*Ccr (**Figure 1B**), including the positive features for CO_2 and HCO_3^-, as well as the negative water band at 3020 cm^{-1} (2280 cm^{-1} in D_2O). However, the kinetic data showed that *Ec*CA catalyses the CO_2/HCO_3^- interconversion about ten times faster compared to *Ks*Ccr, with $\tau_{app} \approx 2$ s for both forward and backward direction (**Figure 2B**).

As control, we tested bovine serum albumin (BSA) and ribulose bisphosphate carboxylase/oxygenase from *Rhodospirillum rubrum* (Rubisco)[23] at pH 8 and comparable protein concentration and hydration levels. BSA, a common biological crowder used here to mimic a generic biological surface[24], shows only residual bicarbonate formation, and the unique water feature is absent in the 'CO_2–N_2' FTIR difference spectrum (**Figure S4**). The reaction of Rubisco with CO_2 resulted in a specific difference spectrum that does not hint at any bicarbonate formation (**Figure S4**). Overall, these controls demonstrated that *Ks*Ccr possesses a 'hidden' CA-like activity similar to the reaction of 'true' CAs.
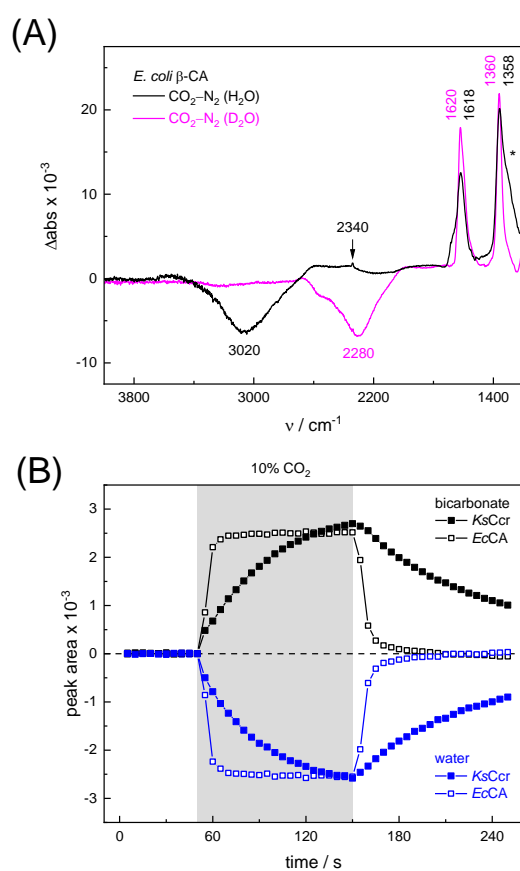

Figure 2 | Infrared characterisation of the reaction of *Ec*CA with CO_2. (A) 'CO_2–N_2' ATR FTIR difference spectra in the presence of H_2O (black) or D_2O (magenta). These data show that *Ec*CA and *Ks*Ccr (**Figure 1B**) react very similar with CO_2. **(B)** Plotting the evolution of spectral traces against time, the superior reaction velocity of *Ec*CA becomes evident.

Substrate Binding and Hydrophilic Residues Influence Anhydrase Activity

In the next step, we investigated the CO_2/HCO_3^- conversion activity of KsCcr in the presence of different compounds, including NADPH, $NADP^+$, native substrate crotonyl-CoA (C-CoA), and side product butyryl-CoA (B-CoA).[7–9] We tested six different combinations: (*i*) KsCcr only, (*ii*) KsCcr + 10 mM $NADP^+$, (*iii*) KsCcr + 10 mM NADPH, (*iv*) KsCcr + 10 mM NADPH + 1 mM C-CoA, (*v*) KsCcr + 1 mM C-CoA, and (*vi*) KsCcr + 1 mM B-CoA. **Figure 3A** shows the HCO_3^- peak area, observed after 60 s in the FTIR difference experiments, *i.e.*, upon saturation of the signals (**Figure S5**), normalized to wild-type KsCcr, which defines '100%' bicarbonate formation. In these experiments, neither NADPH nor $NADP^+$ affected bicarbonate formation of KsCcr, while the presence of C-CoA or B-CoA decreased band intensity by ca. 70% or 85%, respectively. This data suggest that bicarbonate formation and carboxylation of the active enzyme complex are mutually exclusive, indicating that the CO_2/HCO_3^- conversion occurs at the active site of KsCcr.
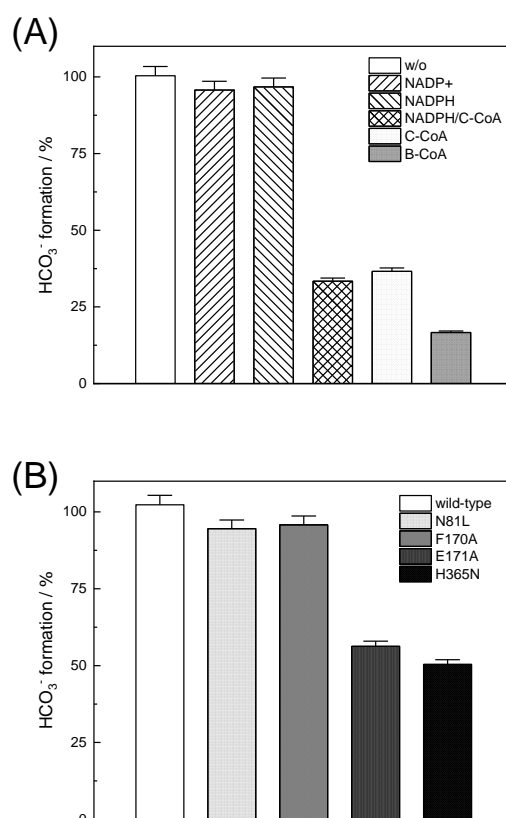

Figure 3 | Bicarbonate formation activity of wild-type KsCcr and variants. (A) The HCO_3^- peak area after 60 s in the presence of CO_2 is set to 100% for wild-type KsCcr and compared for different conditions as annotated in the bar diagram. **(B)** A similar analysis was conducted to compare wild-type KsCcr to four amino acid variants as annotated in the bar diagram.

We previously could show that four amino acids play a key role in CO_2 binding at the active site of *Ks*Ccr: histidine H365, glutamate E171, asparagine N81, and phenylalanine F170.[10] H365 and E171 are involved in coordinating a conserved water molecule in bridging position ('μW'), which is in hydrogen-bonding contact with 3–4 water molecules that connect the active site with bulk water (**Scheme 2B**). Asparagine N81 orients CO_2 in the active site for the carboxylation reaction, and F170 shields the pocket from water. To understand the molecular basis of CO_2/HCO_3^- conversion in *Ks*Ccr, we tested four active site variants in the presence and absence of substrate. In general, the 'CO_2–N_2' FTIR difference spectra of the four variants were all similar to wild-type *Ks*Ccr (**Figure S5**). However, while in the absence of substrate(s), N81L and F170A showed still full bicarbonate formation activity, bicarbonate formation of variants E171A and H365N was reduced by ca. 50% compared to wild-type *Ks*Ccr (**Figure 3B**). All samples were strongly inhibited by C-CoA or B-CoA, in line with the hypothesis that substrate binding suppresses CO_2/HCO_3^- conversion (**Figure S6**). Altogether, these experiments suggested that CA activity depends on the active site of *Ks*Ccr, and likely involves E171 and H365.

Computer simulations reveal conformational dependent CO_2 binding to the active site and explain substrate inhibition

To rationalize the observed inhibition of CA activity through substrate binding, we performed atomistic MD simulations of *Ks*Ccr in presence of CO_2 using the X-ray crystal structure of the enzyme with the NADPH cofactor and B-CoA, the ternary complex (PDB ID 6NA4).[25] Note that the enzyme is a tetramer that shows half-site reactivity, *i.e.*, exists as dimer of closed and open subunits (**Figure 4A**). Compared to the open subunits, the closed subunits contain the substrate and represent the catalytically active sites in the ternary complex. For our simulations, we replaced B-CoA by C-CoA and defined a volume (box in **Figure 4A**) to calculate the CO_2 binding free energy in the open and closed subunit. Notably, active site residues H365 and E171, which we had associated with CA activity (see above), adopted different geometries in the closed and open confirmations. Compared to the open subunit, the distance between E171 and H365 was 3 Å shorter in the closed subunit, and the conserved water molecule μW was hydrogen-bonded between the two residues.
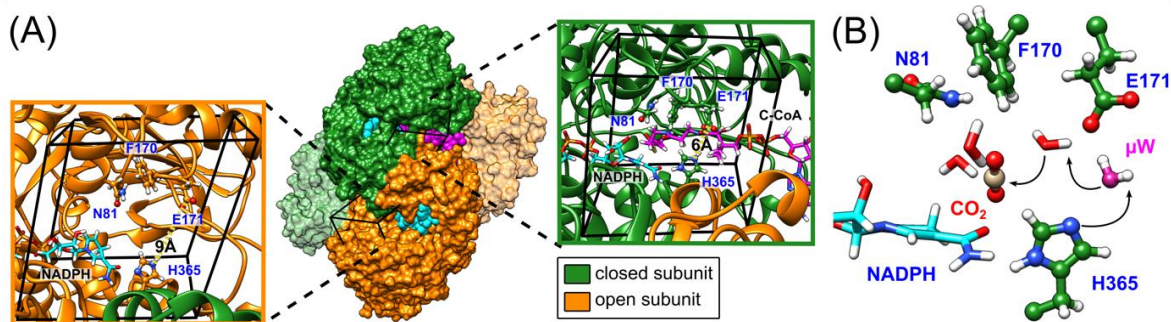
Figure 4 | Computational model and reaction mechanism. (**A**) Crystal structure of *Ks*Ccr (PDB ID 6NA4) in a dimer-of-dimers configuration with open and closed subunits (orange and green, respectively). A close-up to the active site for the open and closed subunit shows the residues N81, F170, E171, and H365. A black box encloses the volume of the active site used to analyse the local CO_2 concentration. NADPH is shown in cyan sticks, C-CoA is shown in magenta sticks. (**B**) Proposed mechanism for CO_2 hydration in the closed active site of the binary complex involving proton transfer from the activated water molecule μW to H365 and nucleophilic attack mediated by hydrogen-bonded water network on CO_2.

For comparison we also studied the X-Ray structure without substrate but with NADPH cofactor (binary complex, PDB ID 6NA4) that presents similar geometries of both residues in closed and open subunits.[25] **Figure 4B** illustrates how H365 can act as base in its neutral, monoprotonated state, initiating proton abstraction from μW, and thus forming the OH^- for subsequent CO_2 hydration. To determine the protonation state of H365 in different subunits of the binary and ternary complexes, we calculated its pK_a shifts.[26] For the open active site, the pK_a shift is negative (ΔpKa = -0.9 ±0.1), indicating that H365 rather adopts a monoprotonated state. For the closed site without substrate (binary complex), we also obtained a negative shift (ΔpK_a = -0.6 ±0.1), while the pK_a was positively shifted in presence of the substrate (ΔpK_a = +1.2 ±0.1), likely because of favorable interactions of the H365 with the negatively charged phosphate groups of C-CoA. Thus, H365 is monoprotonated in the empty closed active site and capable of initiating proton abstraction from μW. In the presence of the substrate, H365 most likely changes its protonation state, thus suppressing CA activity.

In addition, CO_2 binding to the active site also plays an important role. To understand the influence of conformational changes and presence of the substrate on CO_2, we carried out extensive MD simulations. From the ratio of local CO_2 concentration in the active site volume (black box in **Figure 4A**) and the concentration in the bulk we calculated the CO_2 binding free energy to the active site volume for the open and closed subunits of the binary and ternary complexes of *Ks*Ccr ($\Delta G_{bind} = -k_B T ln\left(\frac{c_{act.\,site}}{c_{bulk}}\right)$, see Supporting Information). Our calculations show that the CO_2 binding free energy to the closed subunit with substrate (ternary

complex) is positive whereas the closed subunit in the binary complex without substrate presents the highest CO_2 affinity which makes it more than two times more probable to find a CO_2 molecule in the active site than in the bulk (**Figure 5A**). The open subunit in the ternary complex also shows a significantly increased CO_2 affinity but the distance between E171 and H365 is larger in the open active site, and no bridging water molecule is observed suggesting a diminished catalytic activity.
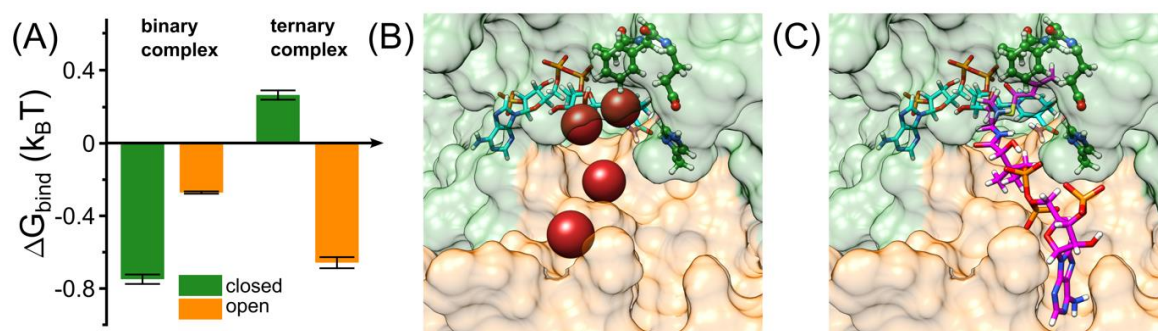

Figure 5 | CO₂ binding in the active site of *Ks*Ccr. (A) Binding free energy (k_BT) of CO_2 in the closed and open subunit of the binary complex with NADPH (PDB ID 6NA6, left) and the ternary complex with NADPH and C-CoA (PDB ID 6NA4, right) from MD simulations. **(B)** Most probable binding sites of CO_2 in the closed active site of the binary complex represented as dark red spheres. **(C)** Representative snapshot of the ternary complex in which the substrate occupies the position of the CO_2 binding sites. NADPH is shown in cyan sticks, C-CoA is shown in magenta sticks and key residues are shown in green sticks.

We then addressed the binding sites of CO_2 in the closed active site without substrate where the affinity is highest. The binding sites connect active site interior and solvent, and the most buried ones are very close to H365, water molecule μW, and E171 (**Figure 5B**). Notably, the substrate in the ternary complex occupies the same positions as the CO_2 binding sites (**Figure 5C**).

In summary, our computer simulations show that the binary complex has a higher CO_2 binding affinity compared to the ternary complex. The CO_2 binding sites in the closed active site are next to H365 and the conserved water molecule μW, so that the monoprotonated form of H365 is able to abstract a proton from μW to form the nucleophilic hydroxyl ion. The absence of NADPH or NADP+ is not expected to affect CO_2 binding or H365 protonation because the coenzyme does not bind directly to the substrate binding site.[25] In contrast, the presence of C-CoA or B-CoA in the ternary complex increases the pK_a of putative proton acceptor H365, thereby eliminating its ability to activate μW water by proton transfer, and simultaneously suppressing CO_2 binding. This can explain the experimentally observed reduction of CA activity and is in line with the fact that the active enzyme ternary complex promotes CO_2 fixation[25], and not CA activity.

Conclusions

In this study, we applied *in situ* ATR FTIR difference spectroscopy and computer simulations to investigate and understand the interaction of crotonyl-CoA carboxylase/reductase (*Ks*Ccr) with CO_2. Our results surprisingly show that *Ks*Ccr possesses a reversible carbonic anhydrase (CA) activity, *i.e.*, CO_2 hydration and HCO_3^- de-hydration. This reaction is strongly suppressed in the presence of C-CoA, the natural substrate of *Ks*Ccr. Extensive MD simulations revealed how C-CoA suppresses CO_2 binding and identified H365 as putative proton acceptor ('base') for CO_2 hydration. Compared to wild-type *Ks*Ccr, variant H365N indeed lacked about 50% CA activity, similar to variant E171A, which forms a hydrogen-bonding complex with H365 through an interstitial, bridging water molecule (μW). The latter is in contact with a chain of water molecules that facilitate contact with bulk water. Upon CO_2 hydration, our FTIR data reveal the loss of a broad band at 3020 cm^{-1} (2280 cm^{-1} in D_2O), which we assign to a strongly hydrogen-bonded water cluster, most likely including μW.

Notably, we also observed very similar spectra for *Ec*CA, which we used as a 'positive control' to validate our experimental setup and confirm our interpretation of *Ks*Ccr's 'hidden' CA activity. *Ec*CA coordinates a zinc cofactor that catalyses the deprotonation of a bound water molecule to a hydroxide ligand (Zn^{2+}-OH^-), promoted by a near-by histidine base (**Scheme 1**). CO_2 reacts with the ligand to HCO_3^-, which is clearly observed in our FTIR difference spectra as a positive contribution. In the following, HCO_3^- leaves the active site and is replaced by another water molecule. Binding of water 're-activates' the cofactor, resulting in a broad negative band in our FTIR difference spectra, similar to what we have observed with *Ks*Ccr. Reported here for the first time, these results establish a unique spectral signature of CA activity, *i.e.*, the IR bands of bicarbonate and a strongly-hydrogen bonded cluster of 'local' water.

The role and importance of a metal ion in CA has been discussed intensively[6]; however, recently Hirakawa *et al.* reported metal-free CAs in cyanobacteria and microalgae that appear to catalyse CO_2 hydration in a purely organic environment.[27] These observations are in line with our experiments on *Ks*Ccr that also suggest metal-free CA activity. Based on our combined experimental and theoretical investigation of CO_2 hydration in *Ks*Ccr, we propose a mechanism related to carbonic anhydrase (**Figure 4B**): (*i*) μW is deprotonated to a bridging hydroxide, μOH^-. The carboxylate side chain of E171 accepts a hydrogen bond from μOH^-, which accepts a hydrogen bond from the imidazole side chain of H356. We speculate that H365 accepts the proton from μW to form the protonated imidazolium cation. (*ii*) Then, μOH^- attacks the carbon

atom of CO_2 to form HCO_3^-. (*iii*) Bicarbonate leaves the active site, potentially triggered by opening of the active site and deprotonation of H365, which is no longer stabilized in the neutral form in the absence of an interstitial water species. This transient opening of the hydrogen-bonding complex will allow intake of CO_2 and cycling between open and closed states is key to catalysis in *Ks*Ccr.[25] (*iv*) Eventually, the binding of another water molecule μW closes the cycle.

Whether *Ks*Ccr reacts as a metal-independent CA under physiological conditions, *e.g.*, 'storing' CO_2 in the absence of substrate, or whether the CA reaction is rather an artefact of the specific experimental setup is subject to future investigation. In any case, we note that our results demonstrate a surprising catalytic plasticity of active sites, according to which a CO_2 binding site for a carboxylation reaction can be alternatively used (or 'exploited') for CO_2 hydration.

Taken together, *in situ* ATR FTIR difference spectroscopy allowed investigating the interaction of different enzymes with CO_2, providing a simple, yet powerful approach to directly identify CA activity for a given biological sample. Moreover, our method is also suited to identify and characterize the source of water and will serve as an important tool to analyze CO_2 hydration in biocatalysis[28–31], homogenous or heterogeneous catalysts[32–34], and (de-)hydration reactions in general.[35,36]

Acknowledgements

References

[1]   R. Wolfenden, *Chem. Rev.* **2006**, *106*, 3379–3396.

[2]   R. J. DiMario, M. C. Machingura, G. L. Waldrop, J. V. Moroney, *Plant Sci.* **2018**, *268*, 11–17.

[3]   D. N. Silverman, R. McKenna, *Acc. Chem. Res.* **2007**, *40*, 669–675.

[4]   V. M. Krishnamurthy, G. K. Kaufman, A. R. Urbach, I. Gitlin, K. L. Gudiksen, D. B. Weibel, G. M. Whitesides, *Chem. Rev.* **2008**, *108*, 946–1051.

[5] C. T. Supuran, *Biochem. J.* **2016**, *473*, 2023–2032.

[6] J. K. Kim, C. Lee, S. W. Lim, A. Adhikari, J. T. Andring, R. McKenna, C. M. Ghim, C. U. Kim, *Nat. Commun.* **2020**, *11*, 1–10.

[7] T. J. Erb, I. A. Berg, V. Brecht, M. Müller, G. Fuchs, B. E. Alber, *Proc. Natl. Acad. Sci.* **2007**, *104*, 10631–10636.

[8] T. J. Erb, V. Brecht, G. Fuchs, M. Müller, B. E. Alber, *Proc. Natl. Acad. Sci.* **2009**, *106*, 8871–8876.

[9] R. G. Rosenthal, M.-O. Ebert, P. Kiefer, D. M. Peter, J. A. Vorholt, T. J. Erb, *Nat. Chem. Biol.* **2014**, *10*, 50–55.

[10] G. M. M. Stoffel, D. A. Saez, H. DeMirci, B. Vögeli, Y. Rao, J. Zarzycki, Y. Yoshikuni, S. Wakatsuki, E. Vöhringer-Martinez, T. J. Erb, *Proc. Natl. Acad. Sci.* **2019**, *116*, 13964–13969.

[11] M. Falk, A. G. Miller, *Vib. Spectrosc.* **1992**, *4*, 105–108.

[12] A. R. Davis, B. G. Oliver, *J. Solution Chem.* **1972**, *1*, 329–339.

[13] W. W. Rudolph, D. Fischer, G. Irmer, *Appl. Spectrosc.* **2006**, *60*, 130–144.

[14] E. Garand, T. Wende, D. J. Goebbert, R. Bergmann, G. Meijer, D. M. Neumark, K. R. Asmis, *J. Am. Chem. Soc.* **2010**, *132*, 849–856.

[15] A. Barth, *Biochim. Biophys. Acta - Bioenerg.* **2007**, *1767*, 1073–1101.

[16] V. A. Lórenz-Fonfria, *Chem. Rev.* **2020**, *120*, 3466–3576.

[17] S. T. Stripp, *ACS Catal.* **2021**, *11*, 7845–7862.

[18] J. Fahrenfort, *Spectrochim. Acta* **1961**, *17*, 698–709.

[19] F. N. Keutsch, R. J. Saykally, *Proc. Natl. Acad. Sci.* **2001**, *98*, 10533–10540.

[20] L. F. Scatena, M. G. Brown, G. L. Richmond, *Science (80-.).* **2001**, *292*, 908–912.

[21] H. Wang, J. C. Wagner, W. Chen, C. Wang, W. Xiong, *Proc. Natl. Acad. Sci.* **2020**, *117*, 23385–23392.

[22] K. S. Smith, F. G. Smith, *FEMS Microbiol. Rev.* **2000**, *24*, 335–366.

[23] H. M. Miziorko, G. H. Lorimer, *Annu. Rev. Biochem.* **1983**, *52*, 507–535.

[24] M. Löwe, M. Kalacheva, A. J. Boersma, A. Kedrov, *FEBS J.* **2020**, *287*, 5039–5067.

[25] H. DeMirci, Y. Rao, G. M. Stoffel, B. Vögeli, K. Schell, A. Gomez, A. Batyuk, C. Gati, R. G. Sierra, M. S. Hunter, E. H. Dao, H. I. Ciftci, B. Hayes, F. Poitevin, P.-N. Li, M. Kaur, K. Tono, D. A. Saez, S. Deutsch, Y. Yoshikuni, H. Grubmüller, T. J. Erb, E. Vöhringer-Martinez, S. Wakatsuki, *ACS Cent. Sci.* **2022**, *8*, 1091–1101.

[26] R. L. Thurlkill, G. R. Grimsley, J. M. Scholtz, C. N. Pace, *Protein Sci.* **2006**, *15*, 1214–1218.

[27] Y. Hirakawa, M. Senda, K. Fukuda, H. Y. Yu, M. Ishida, M. Taira, K. Kinbara, T. Senda, *BMC Biol.* **2021**, *19*, 1–15.

[28] M. L. Zastrow, A. F. A. Peacock, J. A. Stuckey, V. L. Pecoraro, *Nat. Chem.* **2012**, *4*, 118–123.

[29] L. A. Rettberg, M. T. Stiebritz, W. Kang, C. C. Lee, M. W. Ribbe, Y. Hu, *Chem. - A Eur. J.* **2019**, *25*, 13078–13082.

[30] M. Meneghello, A. R. Oliveira, A. Jacq-Bailly, I. A. C. Pereira, C. Leger, V. Fourmond, *Angew. Chemie Int. Ed.* **2021**, *60*, 9964–9967.

[31] D. Shevela, H.-N. Do, A. Fantuzzi, A. W. Rutherford, J. Messinger, *Biochemistry* **2020**, *59*, 2442–2449.

[32] G. Parkin, *Chem. Rev.* **2004**, *104*, 699–768.

[33] L. Koziol, C. A. Valdez, S. E. Baker, E. Y. Lau, W. C. Floyd, S. E. Wong, J. H. Satcher, F. C. Lightstone, R. D. Aines, *Inorg. Chem.* **2012**, *51*, 6803–6812.

[34] S. J. Cobb, V. M. Badiani, A. M. Dharani, A. Wagner, S. Zacarias, A. R. Oliveira, I. A. C. Pereira, E. Reisner, *Nat. Chem.* **2022**, *14*, 417–424.

[35] S. Kobayashi, K. Manabe, *Acc. Chem. Res.* **2002**, *35*, 209–217.

[36] G. Li, B. Wang, D. E. Resasco, *ACS Catal.* **2020**, *10*, 1294–1309.